FILTERING IN MICROCHANNEL HEAT SINK TOPOLOGY OPTIMIZATION

Lacko P.*, Blommaert M., Dekeyser W., and Baelmans M.
*Author for correspondence
Department of Mechanical Engineering,
KU Leuven, Belgium,
E-mail: paul.lacko@kuleuven.be

1 ABSTRACT

In recent years, microchannel heat sinks have increasingly been designed using mathematical approaches such as topology optimization. This tactic can lead to novel heat sink lay-outs with enhanced performance over existing designs. Physics dictate a preference towards very short and small channels for the cooling fluid, benefiting the heat transfer performance. However, the feature size depends on the coarseness of the numerical grid used in the optimization, and very fine designs can simply not be manufactured using existing technologies. In structural optimization, mesh-independent filtering methods are used to ensure grid independence and manufacturability.

In this research, design and sensitivity filtering are tested within liquid cooling microchannel heat sink topology optimization. The optimized designs are evaluated with a focus on the level of grid independence and manufacturability that can be achieved through incorporation of these methods. Additionally, a mutual comparison of both filter methods is performed. Results indicate that for unconstrained optimization problems and under certain conditions relating the filters, it can be proven that both methods will lead to identical results.

2 INTRODUCTION

For many years now, electronic components such as CPUs, graphics cards, and other devices have become increasingly smaller in size and at the same time more powerful in capacity. These devices can only maximize their potential if there is sufficient cooling available to keep them at the required working temperatures for proper operation. To this end, air-cooling devices such as fans are becoming increasingly inadequate and being replaced by liquid cooling alternatives such as microchannel heat sinks.

Research into microchannel heat sinks was initiated by Tuckerman and Pease [1] and the foundation for heat sink topology optimization was laid with the equations derived by Borrvall and Petersson [2]. Since these developments, there have been a rather limited number of research studies on topology optimization specifically applied to different types of heat sinks [3–10]. Finite elements methods are in all cases the numerical method of choice. The presented research uses the work by Van Oevelen [11] as a starting point, where the finite volume method is used to investigate density-based topology optimization applied to pressure-driven microchannel heat sinks.

To date, there are a number of issues that may appear during the optimization process that create a barrier to real world applicability of the optimized heat sink layouts. These problems include numerical instabilities such as checkerboarding, a dependence of optimized layouts on the coarseness of the design grid, and an overall lack of manufacturability of final designs.

These issues are also known in the field of structural topology optimization, and are often tackled by using restriction meth-

NOMENCLATURE

A	[m^2]	Surface area
c	[J/(kg.K)]	Specific heat capacity
F	[-]	Filter matrix
h	[W/(m^2.K)]	Heat transfer coefficient
i	[-]	Index number for cell i
k	[W/(m.K)]	Thermal conductivity
n	[-]	Number of design variables
N_e	[-]	Neighborhood of element e
p	[Pa]	Pressure field
q	[-]	Interpolation parameter
$\dot{Q}$	[W]	Heat transfer rate
R	[m]	Filter radius
T	[K]	Temperature field
v_i	[m^3]	Volume of cell i
$\vec{v}$	[m/s]	Velocity field
w	[-]	Weighting value

Special characters

α	[N.s/m^4]	Inverse permeability
	[-]	Relaxation factor
β	[-]	Steepness of projection function
ε	[-]	Porosity/Controlled field
$\tilde{\varepsilon}$	[-]	Filtered porosity/Physical field
$\bar{\varepsilon}$	[-]	Projected porosity
$\mathcal{J}$	[W]	Cost function
η	[-]	Projection threshold
μ	[Pa.s]	Viscosity
ρ	[kg/m^3]	Density
φ	[-]	State variables
Ω	[-]	Domain

Subscripts

c	Cell center
d	Design filter
diff	Difference
e	Related to cell e
f	Fluid
g	Sensitivity filter
i	Related to cell i
s	Solid
source	Source

ods [12]. Among these methods, mesh-independent filtering methods have proven very popular due to their simplicity in implementation and effectiveness [13].

The present research focuses on the application of mesh-independent filtering methods to microchannel heat sink topology optimization. Concretely, two research questions are studied. Firstly, can the application of mesh-independent filtering methods lead to grid independent optimized designs? Secondly, can these methods ensure manufacturability of optimized designs?

3 MODELING

3.1 Model equations

The steady state Brinkman equations are used to describe the fluid flow through both solid and liquid material. The equations lead to the Stokes flow equations in pure liquid areas and will obey no slip conditions at liquid-solid interfaces. It includes an additional pressure loss term for flows through porous media. The heat transfer model is formulated based on an advection-diffusion equation. The equations are:

$$-\nabla\cdot\mu\nabla\vec{v}+\nabla p+\alpha(\varepsilon)\vec{v}=0\,, \tag{1}$$

$$\nabla\cdot\vec{v}=0\,, \tag{2}$$

$$\nabla\cdot\rho c\vec{v}T-\nabla\cdot k(\varepsilon)\nabla T=0\,, \tag{3}$$

where $\vec{v}$ is the velocity field, p the pressure field, T the temperature field, μ the liquid viscosity, α the material inverse permeability, ρ the liquid density, c the specific heat capacity of the liquid, k the material thermal conductivity, and ε the material porosity. μ, ρ, and c are all constants. α and k are determined by the value of ε and are calculated through interpolation, as follows:

$$\alpha(\varepsilon)=\alpha_s+(\alpha_f-\alpha_s)\varepsilon\frac{1+q}{\varepsilon+q}\,, \tag{4}$$

$$k(\varepsilon)=k_s+(k_f-k_s)\varepsilon\,, \tag{5}$$

where the subscript f denotes the fluid material and s the solid material. q is an interpolation parameter used to discourage the optimization algorithm from retaining intermediate porosity values in optimized designs. This is accomplished by increasingly penalizing the 'mixed phase' between solid and fluid for larger values of q.

3.2 Model approximations

The equations are solved in two dimensions including additional correction terms to account for the third dimension, namely the height of the heat sinks [11]. Additionally, Stokes flow is used for the fluid model based on the assumption of low Reynolds numbers in the fluid subdomain due to the small physical dimensions of the channels that appear in the optimized designs. Variations in the density and viscosity with the temperature are omitted.

Regarding the inverse permeability α, the value α_s for the solid material is ideally equal to infinity. However, high values generate instabilities during the optimization. In practice, α_s is restricted to an intermediate value, corresponding to a material that still allows some throughflow, which contradicts the physics of actual solids. The results of this decision will become apparent in the section 7.

3.3 Optimization problem

The reduced optimization problem is formulated as:

$$\begin{aligned}&\underset{\varepsilon}{\text{minimize}} \quad \mathcal{J}(\varphi(\varepsilon),\varepsilon)=-\dot{Q}=\int_A h(\varepsilon)(T(\varepsilon)-T_{\text{source}})\,\mathrm{d}A\\ &\text{subject to} \quad 0\le\varepsilon\le 1,\ i=1,\dots,n.\end{aligned} \tag{6}$$

where $\varphi=[\vec{v},p,T]$ are the state variables. $\mathcal{J}(\varphi(\varepsilon),\varepsilon)$ is the reduced cost functional, in this case the maximization of the heat transfer from the constant temperature heat source to the cooling fluid. $\varphi(\varepsilon)$ is a solution to the model equations for a given input design ε. ε is the material porosity, which is used as the control variable in the topology optimization problem. The values of the porosity are constrained in each grid cell i between 0 corresponding to solid material, and 1 corresponding to fluid material. n is the number of grid cells.

4 FILTERING METHODS

In essence, filtering methods perform a smoothing operation on a specified variable field to obtain a new variable field with more desirable properties that is subsequently used in the optimization process. Here, we will use a weighted average of variable values around a specified cell or element e as smoothing operation.

To do this, we must first define a neighborhood around the cell e, called N_e [13], as $N_e=\{i|\ \exists\vec{x}_i\in\Omega_i\mapsto||\vec{x}_{c,e}-\vec{x}_i||\le R\}$, where $\vec{x}_{c,e}$ and $\vec{x}_i$ are the spatial locations of the center of cell e and any point within the domain of cell i (Ω_i) respectively, and with R the filter radius. After selecting a value for the filter radius, one can evaluate the neighborhood N_e to determine which cells must be included in the filtering operation for cell e, and this for all cells in the design domain.

There are two classes of filtering methods, namely design- and sensitivity-based methods [12, 13].

4.1 Design filtering

In structural mechanics, design filtering is always called "density" filtering, since the material density is the design variable. However, in heat sink topology optimization, the design variable is the porosity ε. We will also use ε to denote the design variable field in this article.

Design-based filter methods work by modifying the design variable field ε through an averaging operation to create a smoothed design variable field, denoted by $\tilde{\varepsilon}$. This smoothed field is subsequently used to evaluate the design. In other words, ε becomes the controlled field on which design updates occur, and $\tilde{\varepsilon}$ is the actual physical field. $\tilde{\varepsilon}$ is calculated in each optimization iteration based on the values of ε. Mathematically, the

filtered porosity in cell e can be written explicitly as [13, 14]:

$$\tilde{\varepsilon}_e = \frac{\sum_{i \in N_e} w(\vec{x}_i) v_i \varepsilon_i}{\sum_{i \in N_e} w(\vec{x}_i) v_i}, \tag{7}$$

where v_i is the volume and $w(\vec{x}_i)$ the weighting function value for subcell i.

A linearly decaying weighting function is used, $w(\vec{x}_i) = R - ||\vec{x}_{c,e} - \vec{x}_i||$, however other weighting function choices are possible as well [13]. The filtered densities are renormalized to ensure the amount of material before and after filtering remains the same.

After solution of the adjoint model to determine the sensitivity of the cost function with respect to changes in the filtered design, these sensitivities must be modified in a consistent way by applying the chain rule to retrieve the sensitivity with respect to the original controlled porosity values as follows [13]:

$$\frac{\partial \mathcal{J}}{\partial \varepsilon_e} = \sum_{i \in N_e} \frac{\partial \mathcal{J}}{\partial \tilde{\varepsilon}_i} \frac{\partial \tilde{\varepsilon}_i}{\partial \varepsilon_e}, \tag{8}$$

where the first factor in the right-hand side is the cost function gradient, typically calculated with the adjoint approach, and the second factor accounts for the filtering operation and can be derived analytically based on equation 7.

4.2 Projection

Design filtering produces a smoothing effect of the design field. However, this leads to the filtered field taking on intermediate values, which from an optimization point of view is undesirable, because we would like porosity values in the optimized design to be either 0 or 1. In structural topology optimization, this problem is typically handled by incorporating a projection operation after the filtering operation in each optimization step to push the values of the filtered field back to $\{0,1\}$-solutions. A Heaviside step projection formulated as a continuous differentiable function is most often used [15, 16]:

$$\bar{\varepsilon}_e = \frac{\tanh \beta\eta + \tanh \beta(\tilde{\varepsilon}_e - \eta)}{\tanh \beta\eta + \tanh \beta(1 - \eta)}, \tag{9}$$

where $\bar{\varepsilon}$ denotes the projected field, η the threshold location for the projection, and β controls the steepness of the Heaviside step, with $\beta = 0$ corresponding to no projection and $\beta = \infty$ to a discrete step function. As with design filtering, the cost function sensitivity should be modified in a consistent manner to take projection into account. This leads to an equation for the sensitivity similar to equation 8 but with an additional factor, which can be found in [15]. Remark that projection is not always used in conjunction with design filtering, rather it is optional.

4.3 Sensitivity filtering

Sensitivity-based filter methods work by modifying the sensitivities $\nabla \mathcal{J}$ through an averaging operation to create a smoothed sensitivity field, denoted $\widetilde{\nabla \mathcal{J}}$. Mathematically, the filtered sensitivity in cell e can be written explicitly as [17]:

$$\frac{\widetilde{\partial \mathcal{J}}}{\partial \varepsilon_e} = \frac{\sum_{i \in N_e} w(\vec{x}_i) v_i \frac{\partial \mathcal{J}}{\partial \varepsilon_i}}{\sum_{i \in N_e} w(\vec{x}_i) v_i}. \tag{10}$$

This expression is identical to design filtering, equation 7, except for the variable that is being filtered, which is in this case the design sensitivity. Sensitivity filtering is performed after calculation of the design sensitivities, and the filtered sensitivities are fed to the optimization algorithm to determine the design update. In this case, no projection is required to achieve $\{0,1\}$-solutions, since the design field ε that is controlled through optimization is the same as the physical field $\tilde{\varepsilon}$ used to evaluate the designs.

4.4 Differences

There are two main differences between design and sensitivity filtering, excluding projection. First of all, the number of design fields used in the optimization routine differs in both methods. For design filtering, the physical field $\tilde{\varepsilon}$ is derived from the controlled field ε based on the averaging operation, equation 7. The relationship between these two fields can be written as $\tilde{\varepsilon} = f(\varepsilon) = F_d \varepsilon$. Here, $F_d = f(R)$ represents the filter matrix, which can be constructed for a given filter radius R, with the subscript d denoting the design filter. Filtering can be written in such a manner since the weighted averaging is a linear operation.

Sensitivity filtering on the other hand only consists of a single design field ε which doubles as the physical field $\tilde{\varepsilon}$, hence the two fields are equal. Let us denote the adjoint gradient vector by $\nabla \mathcal{J}$. The smoothed sensitivity then becomes

$$\widetilde{\nabla \mathcal{J}} = f(\nabla \mathcal{J}) = F_g \nabla \mathcal{J}, \tag{11}$$

with $F_g = f(R)$ the filter matrix for a given filter radius R, the subscript g standing for gradient (to differentiate from subscript s which previously stood for solid).

The second difference between the two methods is in the application of the constraints. In both cases, the box constraints $[0,1]$ are applied to the controlled field ε. However, since the physical field $\tilde{\varepsilon}$ is used to evaluate the cost function and hence design performance, it is only logical that this field should in fact lie within the box constraints. As previously stated, $\varepsilon = \tilde{\varepsilon}$ for the sensitivity filter, hence the constraints are applied to the desired field.

This is not the case with the design filter, and application of the box constraints to the controlled field ε will lead to intermediate porosity values in the physical field $\tilde{\varepsilon}$. This also explains why projection is often applied when using design filtering to obtain discrete $\{0,1\}$-solutions.

4.5 Equivalence

A third research question presents itself: can we obtain the same optimized design through design and sensitivity filtering, irrespective of which method we use? For this to be the case, we

can postulate the following. Suppose we start from an initial design ε^0 with corresponding initial cost function value $\mathcal{J}(\varepsilon = \tilde{\varepsilon}^0)$ evaluated based on the physical field. In order for design and sensitivity filtering to remain equal after an optimization step with new cost function value $\mathcal{J}$, the design fields used to evaluate the cost function must be identical.

Assume for the following derivation that an unconstrained steepest descent optimization algorithm is used. For the sensitivity filter, the new design field $\tilde{\varepsilon}_g^{\text{new}}$ can be written as:

$$\tilde{\varepsilon}_g^{\text{new}} = \tilde{\varepsilon}_g^0 - \alpha_g \widetilde{\nabla \mathcal{J}}\,, \tag{12}$$

where $\tilde{\varepsilon}_g^0$ is the physical field from the previous iteration, α_g is a relaxation factor on the optimization step, and $\widetilde{\nabla \mathcal{J}}$ the sensitivity-filtered adjoint gradient used in the optimization step. Using equation 11, this can be rewritten into

$$\tilde{\varepsilon}_g^{\text{new}} = \tilde{\varepsilon}_g^0 - \alpha_g F_g \nabla \mathcal{J}\,. \tag{13}$$

For the design filter, the new design field $\tilde{\varepsilon}_d^{\text{new}}$ can be written as:

$$\tilde{\varepsilon}_d^{\text{new}} = F_d(\varepsilon_d^0 - \alpha_d \nabla_\varepsilon \mathcal{J})\,. \tag{14}$$

$\nabla_\varepsilon \mathcal{J}$ is the gradient with respect to the original design field ε. For optimization problems where all design variables are also degrees of freedom and regular numerical grids, the filter matrix F_d is square and symmetric, and the gradient equation 8 can in fact be rewritten as:

$$\nabla_\varepsilon \mathcal{J} = F_d \nabla \mathcal{J}\,. \tag{15}$$

Substituting this relation into equation 14 for the new design field and expanding, leads to:

$$\tilde{\varepsilon}_d^{\text{new}} = F_d \varepsilon_d^0 - \alpha_d F_d F_d \nabla \mathcal{J}\,. \tag{16}$$

Comparing equations 13 and 16 for the new physical design field after an optimization step and equating terms leads to the following conclusion: design and sensitivity filtering produce identical results, if and only if:

1. The initial physical design fields before an optimization step are equal: $\tilde{\varepsilon}_g^0 = F_d \varepsilon_d^0$.
2. The optimization step relaxation factors are equal: $\alpha_g = \alpha_d$.
3. The filter matrices are related by: $F_g = F_d F_d$.

Additionally, the adjoint gradient $\nabla \mathcal{J}$ must be equal in both cases, but this will always be satisfied if the initial physical design field condition is the same. The above derivation corresponds to an unconstrained optimization algorithm using the method of steepest descent. Addition of constraints leads to a final condition:

4. The constraints must be applied to the physical porosity field: $0 \leq \tilde{\varepsilon} \leq 1$.

This last condition changes nothing for sensitivity filtering, but shifts the constraints in design filtering from the controlled field ε to the physical field $\tilde{\varepsilon} = F_d \varepsilon$.

5 NUMERICAL IMPLEMENTATION

The model equations are discretized using a finite volume method and implemented in an in-house topology optimization framework using MATLAB. The state variables are calculated on a staggered, Cartesian grid. The adjoint model equations are derived using the continuous adjoint method.

For the optimization algorithm, both the method of moving asymptotes (MMA) [18] as well as linear programming with L_2-regularization using *quadprog* from the MATLAB standard optimization toolbox were used. The optimization problem is solved using a nested approach, where in each optimization iteration the state and adjoint equations are satisfied.

The filtering schemes were implemented using explicit formulations as provided in section 4. In order to perform the filtering operation near the boundaries of the domain, the variables that are filtered are extended outside of the domain according to a Neumann boundary condition by creating a mirrored field. The cell weighting values are calculated using numerical integration over the cells within the neighborhood matrix.

6 PROBLEM SETUP

The design domain is a 1 cm by 1 cm square surface. The north and south border correspond to adiabatic walls and the west and east border are the fluid inlet and outlet respectively. A fixed overall (static) pressure drop of 10 kPa over the heat sink is assumed and used as the inlet and outlet boundary conditions. The solid material corresponds to silicon, and water is assumed for the liquid. All material and parameter values are the same as in chapter 6 of Van Oevelen [11], except for the interpolation factor q. Typically, q is gradually increased throughout optimization to avoid getting stuck in local optima. In this work however, it is kept constant at a reasonably low value $q = 1$ for algorithmic comparison purposes. The domain is discretized into 800x800 cells. When using linear programming, the scale factor for the L_2-regularization term is equal to 100.

Regarding the filter methods, the filter radius is equal to 100 μm with linear weighting in all cases. Assuming deep reactive ion etching is used to fabricate the microchannel heat sinks, this filter radius corresponds to a manufacturable channel size that currently is easily achievable. Consequently, we would like any optimized designs to not contain features smaller in size than the selected filter radius.

In cases when projection is used, the Heaviside step threshold η is set at 0.5 and the steepness parameter $\beta = 6$. Selecting a value for the steepness involves a trade-off between incomplete projection back to $\{0,1\}$-solutions for low values of β and numerical instabilities in the optimization for high values. The value used here is on the conservative side so as to not disturb the optimization.

7 OPTIMIZATION RESULTS

7.1 MMA

Figure 1 shows an optimized design without the use of a filter. Black corresponds to solid walls, white to fluid-containing channels. The fluid inlet is on the left and outlet on the right. It is immediately clear that this design contains a large amount of very short and fine channels that, while beneficial for the heat transfer to the fluid, are not readily manufacturable.

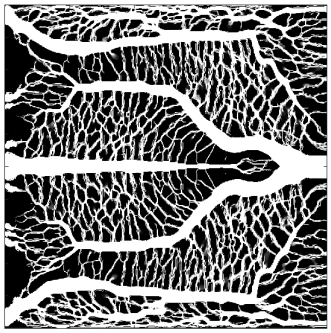

Figure 1. Optimized design without using a filter.

Figure 2 shows an optimized design using a design filter. The effect of the filter is recognizable in the fact that the number of very small channels and fine features is greatly reduced. However, there still are a few narrow channels that would fall outside of the manufacturing constraints. Another observation is the lack in connectivity between inlet and outlet channels, this is due to the low value used for the solid inverse permeability α_s.

As mentioned in section 4, design filtering tends to push the porosity towards intermediate values. Sigmund [13] used the measure of non-discreteness as a monitoring criterion to quantify how much gray is in an optimized design, $M_{nd} = \frac{4}{n}\sum_{i=1}^{n}\tilde{\varepsilon}_i(1-\tilde{\varepsilon}_i)$ x 100%, with a value of 0% corresponding to a fully discrete design and 100% to a design that is completely gray. For the optimized design without filtering, $M_{nd} = 8.45\%$, which is already a relatively large value. Using design filtering, this value increases to $M_{nd} = 21.59\%$. To mitigate the increase in gray in the optimized designs, projection can be used, the results of which are shown in figure 3.

Projection decreases the measure of non-discreteness to $M_{nd} = 12.71\%$. This value is not as low as the optimized design without filtering, confirming that the selected value for the projection steepness β is not large enough.

Figure 4 shows an optimized design using a sensitivity filter. The measure of non-discreteness in this case is $M_{nd} = 1.54\%$. Again, similarities exist in optimized layout when comparing the sensitivity filter to the design filter. However, using sensitivity filtering, a much larger portion of the optimized designs consists of channels. This observation can also be linked to the value used for α_s, with additional simulations showing a rather unintuitive positive correlation between α_s and the amount of white in optimized designs.

In order to determine if grid independence can be achieved by using filtering, a number of designs were optimized on varying grid sizes between 50x50 and 800x800. Analysis of the results showed that there were still considerable variations in the optimized design topologies, indicating that grid independence is not quite achieved with these methods. However, there are indications that the studied optimization problem is non-convex with a large number of local minima. Our research suggests that MMA is not particularly suited towards handling this type of problem, and an alternative optimization algorithm should be used, if grid independence were to be pursued.

7.2 Linear Programming

In order to demonstrate the equivalence between design and sensitivity filtering under the conditions provided in section 4.5, a number of optimization simulations were run on a 50x50 grid, and the design fields in each iteration were compared. To quantify the difference between the filtering methods, the root mean square (RMS) difference between the design fields $\mathrm{RMS}_{\mathrm{diff}} = \sqrt{\frac{1}{n}\sum_{i=1}^{n}(\varepsilon_{d,i}-\varepsilon_{g,i})^2}$ was calculated and plotted for each optimization iteration. The results can be seen in figure 5.

'LP default' depicts the RMS difference using *quadprog* with default values for the optimization settings. 'LP high tol' is the same simulation with the *OptimalityTolerance* parameter set to 10^{-12}. For comparison, the RMS difference using MMA for both design and sensitivity filtering has been plotted as well.

Figure 5 confirms the similarity in design fields using both filter methods, until the point where the constraints become active, occurring after the 73rd iteration (denoted with the solid black line). Beyond this point, the physical design fields $\tilde{\varepsilon}$ from both filter methods start diverging. Using MMA with the constraints applied to the controlled fields ε, optimization results almost immediately diverge, as should be expected.

8 CONCLUSION AND FUTURE WORK

In this research we have applied design and sensitivity filtering to topology optimization of microchannel heat sinks. Results indicated that grid independence cannot be achieved using these filter methods alone. These methods do go some way towards ensuring manufacturability, however there is no direct relation between the filter parameters in the optimization and actual manufacturing constraint values such as smallest producible channel width, which means manufacturability cannot be guaranteed for any given design. Finally, it has been shown that for unconstrained optimization, design and sensitivity filtering can produce identical optimized designs under certain conditions, indicating an equivalence between these methods.

Further research into a comparison of the filter methods including constraints and the search for a possible equivalence for these conditions is ongoing. Besides that, there are a number of shortcomings in the modeling, such as the parameterization of the solid material and too low value for α_s resulting in non-connectivity, and in the optimization algorithm MMA, where local optima are an issue. Both of these issues will be tackled in the near future as well, by looking into more suitable parameterization methods and optimization algorithms.

Figure: Optimized designs using various filters.

Figure 2. Design filter.

Figure 3. Design filter with projection.

Figure 4. Sensitivity filter.

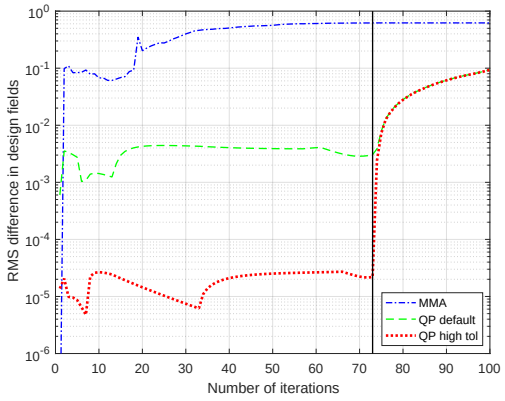

Figure 5. RMS-difference in design field for various optimization algorithms.

ACKNOWLEDGMENT

The author would like to thank the Agency for Innovation by Science and Technology in Flanders (IWT) for their financial support through a research grant no. 151388.

REFERENCES

[1] Tuckerman D. B., and Pease R. F. W., High-performance heat sinking for VLSI, *IEEE Electron Device Letters* , Vol. 2, No. 5, pp. 126-129, May 1981.

[2] Borrvall T., and Petersson J., Topology optimization of fluids in Stokes flow, *International Journal for Numerical Methods in Fluids*, Vol. 41, No. 1, pp. 77-107, Jan. 2003.

[3] Bruns T. E., Topology optimization of convection-dominated, steady-state heat transfer problems, *International Journal of Heat and Mass Transfer*, Vol. 50, No. 15-16, pp. 2859-2873, Jul. 2007.

[4] Yoon G. H., Topological design of heat dissipating structure with forced convective heat transfer, *Journal of Mechanical Science and Technology*, Vol. 24, No. 6, pp. 1225-1233, Jun. 2010.

[5] Dede E. M., Optimization and Design of a Multipass Branching Microchannel Heat Sink for Electronics Cooling, *Journal of Electronic Packaging*, Vol. 134, p. 41001-1-10, Dec. 2012.

[6] Koga A. A., Lopes E. C. C., Villa Nova H. F., de Lima C. R., and Silva E. C. N., Development of heat sink device by using topology optimization, *International Journal of Heat and Mass Transfer*, Vol. 64, pp. 759-772, Sep. 2013.

[7] Yaji K., Yamada T., Kubo S., Izui K., and Nishiwaki S., A topology optimization method for a coupled thermal-fluid problem using level set boundary expressions, *International Journal of Heat and Mass Transfer*, Vol. 81, pp. 878-888, Feb. 2015.

[8] Dede E. M., Joshi S. N., and Zhou F., Topology Optimization, Additive Layer Manufacturing, and Experimental Testing of an Air-Cooled Heat Sink, *Journal of Mechanical Design*, Vol. 137, pp. 111403-1-9, Nov. 2015.

[9] Zhou M., Alexandersen J., Sigmund O., and Claus C. B., Industrial application of topology optimization for combined conductive and convective heat transfer problems, *Structural and Multidisciplinary Optimization*, Vol. 54, No. 4, pp. 1045-1060, Apr. 2016.

[10] Alexandersen J., Sigmund O., and Aage N., Large scale three-dimensional topology optimisation of heat sinks cooled by natural convection, *International Journal of Heat and Mass Transfer*, Vol. 100, pp. 876-891, Sep. 2016.

[11] Van Oevelen T., Optimal Heat Sink Design for Liquid Cooling of Electronics, *PhD thesis*, KU Leuven, 2014.

[12] Sigmund O. and Maute K., Topology optimization approaches: A comparative review, *Structural and Multidisciplinary Optimization*, Vol. 48, No. 6. pp. 1031-1055, Dec. 2013.

[13] Sigmund O., Morphology-based black and white filters for topology optimization, *Structural and Multidisciplinary Optimization*, Vol. 33, No. 4-5, pp. 401-424, Feb. 2007.

[14] Bruns T. E., and Tortorelli D. A., Topology optimization of nonlinear elastic structures and compliant mechanisms, *Computer Methods in Applied Mechanics and Engineering*, Vol. 190, No. 26-27, pp. 3443-3459, Mar. 2001.

[15] Xu S., Cai Y., and Cheng G., Volume preserving nonlinear density filter based on heaviside functions, *Structural and Multidisciplinary Optimization*, Vol. 41, No. 4, pp. 495-505, Apr. 2010.

[16] Wang F., Lazarov B. S., and Sigmund O., On projection methods, convergence and robust formulations in topology optimization, *Structural and Multidisciplinary Optimization*, Vol. 43, No. 6, pp. 767-784, Jun. 2011.

[17] Sigmund O., Design of multiphysics actuators using topology optimization - Part II: Two-material structures, *Computer Methods in Applied Mechanics and Engineering*, Vol. 190, No. 49-50, pp. 6605-6627, Oct. 2001.

[18] Svanberg K., The method of moving asymptotes-a new method for structural optimization, *International Journal for Numerical Methods Engineering*, Vol. 24, No. 2, pp. 359-373, Feb. 1987.